Journal of Atomic, Molecular, Condensed Matter & Nano Physics
Vol. 7, No. 3, pp. 175–188, 2020
ISSN 2582-8215 (online)
Published by RGN Publications
DOI: 10.26713/jamcnp.v7i3.1543

http://www.rgnpublications.com

Proceedings of ICACTCE'21
High School of Technology, Moulay Ismail University Meknes, Morocco, and
Faculty of Sciences and Techniques Mohammedia, Hassan II University, Morocco
March 24 – 26, 2021, Morocco
***Editors*:** Mariyam Ouaissa, Mariya Ouaissa, Sarah El Himer, and Zakaria Boulouard

Research Article

Lattice Boltzmann Simulations of Coupled Mixed Convection and Radiation Effect in a Two-Sided Lid-Driven Enclosure

Youssef Dahani*, Mohammed Hasnaoui, Abdelkhalek Amahmid, Ismail Filahi, Abdelmajid Mansour and Safae Hasnaoui

LMFE, Department of Physics, Cadi Ayyad University, Faculty of Sciences Semlalia, B.P. 2390, Marrakesh, Morocco

Abstract. Using *Lattice Boltzmann Method* (LBM), the mixed convection and surface radiation effect in a two-sided lid-driven square cavity is studied numerically with air as a working fluid. The numerical code is validated against results available in the literature. The parameters governing the problem are the emissivity of the walls, the Reynolds number and the Richardson number that was varied through the Grashof number. The results obtained show significant effects of the Richardson number and surface radiation on the overall structure of the flow and heat transfer characteristics. The contribution of radiation component to the total Nusselt number outclasses that of convection for high emissive walls at some threshold value of Richardson number.

Keywords. Mixed convection; Double-lid driven-cavity; Surface radiation; Lattice-Boltzmann method

PACS. 47.55.pb; 44.25.+f; 44.40.+a

1. Introduction

Fluid flows and heat transfers in closed cavities that are mechanically driven by tangential motions of the walls, represent a fundamental problem in fluid mechanics and heat transfer.

*Corresponding author: youssef.dahani@uca.ac.ma

This kind of problems have many applications in engineering, due to their fundamental nature and relevance for various engineering applications, such as float glass production, solar collectors, cooling of electronic devices, thermal–hydraulics of nuclear reactors, dynamics of lakes, materials processing, and many others.

The lid-driven cavity has attracted the attention of researchers since the early 1960s [16] . Due to the limitation of computing resources at that earliest stage of research, the experimental method was the main mean of investigation. Koseff and Street [12], and Prasad and Koseff [21] have conducted comprehensive studies on the subject. Other experimental contributions by Migeon *et al*. [15], Ilegbusi and Mat [10], and Vogel *et al*. [22] provided significant impetus to research on lid-driven cavities. The literature review shows that mixed convection flows in lid-driven cavities is a subject of interest of several researchers worldwide. For instance, Guo *et al*. [8] used the lattice Boltzmann method to simulate mixed convection in a lid-driven cavity for various aspect ratios. They observed a mixed convection regime when the Richardson number is of order of unity. Likewise, they developed an analytical expression based on the scale analysis to evaluate the effect of the aspect ratio on the average Nusselt number in dominating forced convection regime. On his side, Nasrin [19] examined the influence of the governing physical parameters on mixed convection in a horizontal lid-driven cavity with an undulating base surface. He reported that the use of a wavy lid-driven cavity could lead to an effective heat transfer mechanism at larger wavy surface amplitudes. More recently, Perumal [20] used the lattice Boltzmann method to study fluid flows generated in a double-sided rectangular cavities and reported the existence of multiple fluid flow solutions above some threshold value of Reynolds number.

The combined effects of mixed convection and radiation on the flow characteristics and heat transfer in lid-driven cavities is very poorly documented in the literature review. Balaji *et al*. [3] investigated the effect of surface radiation on laminar mixed convection induced in a two-dimensional, differentially heated lid-driven cavity. They reported that, even in the full mixed convection regime, radiation contribution to the total heat transfer can be as high as 64%. A similar problem was examined by Belmiloud and Chemloul [4]. Their results show that radiation affects considerably both components of the total heat transfer. On their side, Antar *et al*. [2] investigated the effect of thermal radiation on heat transfer in a lid-driven cavity heated from below and having an aspect ratio $A = 10$. In their study, a variable speed was considered for the moving boundary. They concluded that, under laminar conditions, thermal radiation plays a significant role in heat transfer characteristics of the lid-driven cavity. Results concerning the importance of radiation in the case of lid-driven cavities filled with radiative emitting, absorbing and scattering gray media, were reported in the numerical works by Mohammadi and Nassab [17], and Mahapatra [14].

In most of studies available in the literature on lid-driven cavities, combined effects of surface radiation and mixed convection have been ignored and remain still not enough addressed. Therefore, the present study is dedicated to the examination of this ignored coupling in a two-sided lid-driven cavity. A parametric study is carried out while varying the Richardson number and the emissivity of the walls. The combined effects of the latters on fluid flow and heat transfer characteristics are scrutinized.

2. Mathematical Formulation

2.1 Problem Statement

The geometry of the present problem is shown in Figure 1. It consists of a two-dimensional square cavity having a height H'. The right vertical wall of constant temperature T_h (heated wall), and the left vertical one of constant temperature T_c (cooled wall) are both driven upwards with the same velocity v_0. The cavity is insulated through its horizontal walls and filled with air as a coolant fluid ($Pr = 0.71$). The inner surfaces of the cavity, in contact with the fluid, are assumed to be gray, diffuse emitters and reflectors of radiation.

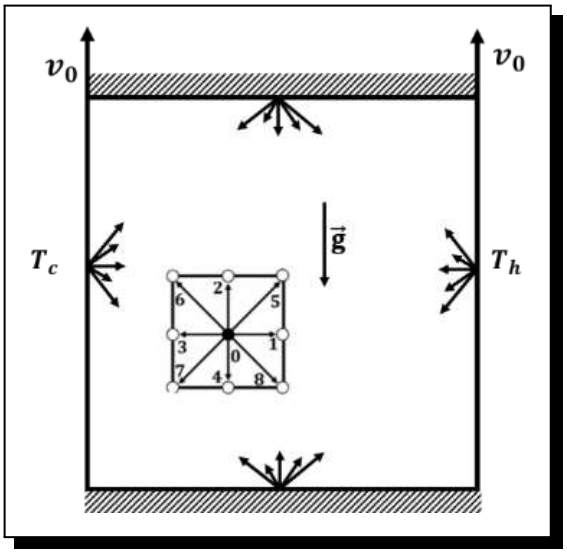

Figure 1. Schematic diagram of the studied configuration and lattices disposition within the cavity for the D2Q9 arrangements

2.2 Lattice-Boltzmann Method

The Boltzmann method is derived from LGA (Lattice-Gas-Automata) method that models a fluid at the microscopic level. In this approach, the fluid is considered as a population of particles,localized on the nodes of a given grid and moving along the links of the network. The problem studied is governed by the Boltzmann equations, eqs. (2.1) and (2.2), which are written in the Bhatnagar-Gross-Krook (BGK) approximation [5]. The Lattice-Boltzmann equation in the presence of an external force F can be used both for flow and temperature fields as follows:

$$f_k(r + c_k\Delta t, t + \Delta t) = f_k(r,t) - \frac{1}{\tau_f}\cdot(f_k(r,t) - f_k^{eq}(r,t)) + F_k\Delta t\,, \tag{2.1}$$

$$g_k(r + c_k\Delta t, t + \Delta t) = g_k(r,t) - \frac{1}{\tau_g}\cdot(g_k(r,t) - g_k^{eq}(r,t))\,. \tag{2.2}$$

The parameters τ_f, τ_g and Δt represent the flow relaxation time, the relaxation time of temperature and linkage time, respectively. It is anticipated that the studied system evolves from a given state of disequilibrium to another where the thermodynamic equilibrium is recovered. During its evolution to wards the equilibrium state, the system is governed by two relaxation times (τ_f and τ_g). The Boltzmann equations (2.1) and (2.2) describe the evolution

of the distribution functions both in time and space. The Maxwell distribution functions, characterizing the local dynamic and thermal equilibrium are $f_k^{eq}(r,t)$ and $g_k^{eq}(r,t)$, respectively. They are given by the following relations [18]:

$$f_k^{eq}(r,t) = \omega_k \rho \left[1 + 3\frac{\vec{c}_k \cdot \vec{u}}{c^2} + \frac{9}{2}\frac{(\vec{c}_k \cdot \vec{u})^2}{c^4} - \frac{3}{2}\frac{\vec{u} \cdot \vec{u}}{c^2}\right], \tag{2.3}$$

$$g_k^{eq}(r,t) = \omega_k T \left[1 + 3\frac{\vec{c}_k \cdot \vec{u}}{c^2}\right]. \tag{2.4}$$

In the previous equations, $\vec{u}$ and ρ denote the speed and macroscopic density, respectively. The D_2Q_9 model for flow and temperature is used in the present study. For this model, the discrete velocities, $\vec{c}_k$, are defined as follows [23]:

$$\vec{c}_k = c\begin{cases} 0 & \text{for } k = 0, \\ \left(\cos\left[(k-1)\frac{\pi}{2}\right], \sin\left[(k-1)\frac{\pi}{2}\right]\right), & \text{for } k = 1,2,3,4, \\ \sqrt{2}\left(\cos\left[(k-5)\frac{\pi}{2} + \frac{\pi}{4}\right], \sin\left[(k-1)\frac{\pi}{2} + \frac{\pi}{4}\right]\right), & \text{for } k = 5,6,7,8. \end{cases} \tag{2.5}$$

The weighting factor, ω_k, is given by:

$$\omega_k = \begin{cases} 4/9, & k = 0, \\ 1/9, & k = 1,2,3,4, \\ 1/36, & k = 5,6,7,8, \end{cases} \tag{2.6}$$

The Boussinesq approximation is introduced in the discrete external force using the following expression [13]:

$$F_k = 3\omega_k \rho g \beta (T - T_0) \cdot c_{ky}, \tag{2.7}$$

where $T_0 = (T_h + T_c)/2$, β is the thermal expansion coefficient and c_{ky} is the projection of the microscopic velocity $\vec{c}_k$ on the y axis.

The non-slip and impermeability on the rigid boundaries have been satisfied by using classical bounce-back boundary conditions on the rigid walls of the cavity. In the streaming step, all the functions oriented to the exterior of the cavity are determined. After the collision with the rigidwalls, the functions oriented to the interior of the cavity are unknown. They are determined by using the values of the functions mirror; those oriented to the exterior.

It is to underline that simple bounce-back issued on all the cavity's walls except the right moving one, where the particle distribution functions were calculated using similar boundary conditions to those proposed by Zou and He [25].

The particles density distribution functions on the rigid walls of the cavity are obtained as follows:

$$\begin{cases} f_2 = f_4,\ f_5 = f_7 \text{ and } f_6 = f_8, & \text{(bottom wall)}, \\ f_4 = f_2,\ f_7 = f_5 \text{ and } f_8 = f_6, & \text{(top wall)}. \end{cases} \tag{2.8}$$

The vertical component of velocity on the left and right moving boundaries, the fluid density and the particles distribution functions, are evaluated as follows:

On the left boundary:

$$\begin{cases} v = v_0, \\ \rho = f_0 + f_2 + f_4 + 2(f_3 + f_6 + f_7), \\ f_1 = f_3, \\ f_5 = f_7 - \dfrac{1}{2}(f_2 - f_4) + \dfrac{1}{2}\rho v_0, \\ f_8 = f_6 + \dfrac{1}{2}(f_2 - f_4) - \dfrac{1}{2}\rho v_0 . \end{cases} \tag{2.9}$$

On the right boundary:

$$\begin{cases} v = v_0, \\ \rho = f_0 + f_2 + f_4 + 2(f_1 + f_5 + f_8), \\ f_3 = f_1, \\ f_7 = f_5 + \dfrac{1}{2}(f_2 - f_4) - \dfrac{1}{2}\rho v_0, \\ f_6 = f_8 - \dfrac{1}{2}(f_2 - f_4) + \dfrac{1}{2}\rho v_0 . \end{cases} \tag{2.10}$$

Now, concerning the thermal boundary conditions on the horizontal adiabatic walls(bottom and top walls), the following expressions were used [7]:

$$\begin{cases} g_{k,0} = \dfrac{4g_{k,1} - g_{k,2} - 2dy\omega_k N_r Q_r}{3}, & k = 0,\ldots,8, \\ g_{k,n} = \dfrac{4g_{k,n-1} - g_{k,n-2} - 2dy\omega_k N_r Q_r}{3}, & k = 0,\ldots,8. \end{cases} \tag{2.11}$$

On the left and right driven walls, the temperatures are known, which leads to the following relations:

$$\begin{cases} g_1 = T_c \cdot (\omega_1 + \omega_3) - g_3 \\ g_5 = T_c \cdot (\omega_5 + \omega_7) - g_7 \\ g_8 = T_c \cdot (\omega_6 + \omega_8) - g_6 \end{cases} \quad \text{(for the left wall)}, \tag{2.12}$$

$$\begin{cases} g_3 = T_h \cdot (\omega_1 + \omega_3) - g_1 \\ g_7 = T_h \cdot (\omega_5 + \omega_7) - g_5 \\ g_6 = T_h \cdot (\omega_6 + \omega_8) - g_8 \end{cases} \quad \text{(for the right wall)} \tag{2.13}$$

Then, the macroscopic quantities which are the density, ρ, the velocity $\vec{u}$, and the temperature, T, can be obtained by using the following formulas:

$$\begin{cases} \rho(r,t) = \sum\limits_{k=0}^{k=8} f_k(r,t), \\ \rho\vec{u}(r,t) = \sum\limits_{k=0}^{k=8} \vec{c}_k f_k(r,t), \\ T(r,t) = \sum\limits_{k=0}^{k=8} g_k(r,t). \end{cases} \tag{2.14}$$

The kinematic viscosity, ν, and the thermal diffusivity, α, are linked to the relaxation times using the Chapman-Enskog procedure [6], which leads to:

$$\nu = (\tau_f - 0.5)c_s^2\Delta t \quad \text{and} \quad \alpha = (\tau_g - 0.5)c_s^2\Delta t . \tag{2.15}$$

2.3 Radiation Equations

The use of the net-radiation method for an enclosure, allows to derive an expression linking the localized heat flux due to the radiative heat transfer and the surface temperature of a given wall. The walls of the cavity were divided into $N = 640$ elementary segments for the considered grid (160×160). Each of these segments is satisfactorily small to be considered isothermal. The view factors between the isothermal elementary surfaces were determined by the Hottel's [9] crossed string method, taking care to check that the view factors summation equals unity for each surface. The calculation of the radiative heat exchange between the cavity walls is based on the radiosity method. In the case of a radiatively non-participating medium, the non-dimensional radiosity equation for the ith element of the enclosure may be calculated as:

$$J_i = \varepsilon_i \left(\frac{T_i}{\theta_0} + 1 \right)^4 + (1 - \varepsilon_i) \sum_{j=1}^{N} F_{ij} J_j \,. \tag{2.16}$$

The dimensionless net radiative heat flux leaving an element of surface S_i is evaluated by:

$$Q_r = \varepsilon_i \left[\left(\frac{T_i}{\theta_0} + 1 \right)^4 - \sum_{j=1}^{N} F_{ij} J_j \right] . \tag{2.17}$$

2.4 Numerical Validation and Grid Size Effect

The numerical code was validated in the absence of radiation against available results in the literature in the case of mixed convection induced in a one-sided lid-driven cavity [1, 11] and in the presence of radiation by considering coupling between natural convection and surface radiation in a closed cavity [24]. A uniform grid of 160×160 was used in the present study. The comparative results are presented in Table 1 (mixed convection in a lid-driven cavity) and Table 2 (natural convection coupled with radiation) for air as a working fluid. In the case of mixed convection, the results presented in Table 1 in terms of average Nusselt number, show that our code reproduces with a good agreement the results reported in refs. [1, 11]; the maximum difference being within 5.8%. Also, in the presence of radiation, it can be seen from Table 2 that the comparative results, in terms of Nu_{Cv}, Nu_{Rd} and Nu, against those obtained by Wang *et al*. [24] are in very good agreement; the maximum difference being within 0.3%.

Table 1. Validation of the numerical code in the case of the lid driven cavity for $Re = 100$

Gr	Present	Ref. [11]	Ref. [1]
10^2	2.0518	1.94 5.8%	2.02 1.6%
10^4	1.4085	1.34 5.1%	1.38 2%
10^6	1.0317	1.02 1.1%	1.02 1.1%

Table 2. Validation of the numerical code for $Ra = 10^6$, $\varepsilon = 0.8$, $T'_0 = 293.5\,\mathrm{K}$ and $\Delta T' = 10\,\mathrm{K}$

	Nu_{Cv}	Nu_{Rd}	Nu
Wang *et al.* [24]	7.815	11.265	19.080
LBM results	7.8346	11.2492	19.0839
Relative difference	0.3%	0.1%	0.02%

2.5 Heat Transfer

The average normalized convective and radiative Nusselt numbers, calculated along the left vertical heated wall, are respectively calculated as:

$$Nu_{Cv} = \int_{\text{wall}} \left.\frac{\partial\theta}{\partial Y}\right|_{Y=0} dX \tag{2.18}$$

and

$$Nu_{Rd} = \int_{\text{wall}} N_r Q_r|_{Y=0}\, dX\,, \tag{2.19}$$

where N_r is the convection-radiation number and Q_r the dimensionless radiative heat flux.

The total average Nusselt number is obtained by summing the convective and radiative components:

$$Nu = Nu_{Cv} + Nu_{Rd}\,. \tag{2.20}$$

3. Results and Discussion

This study is conducted for the Richardson number, Ri and the emissivity of the walls, ε, varying respectively in the ranges $0.01 \le Ri \le 100$ and $0 \le \varepsilon \le 1$. It was varied through the Grashof number, Gr ($100 \le Gr \le 10^6$) since the value of Re was set at 100. The results obtained are illustrated in terms of streamlines, isotherms, vertical velocity and temperature profiles at mid-height of the cavity and averaged Nusselt numbers.

3.1 Fluid Flow and Temperature Fields

Typical stream lines and isotherms, characterizing respectively the flow structure and the temperature distribution inside the cavity, obtained numerically for various Richardson number for $\varepsilon = 0$ and 1 are illustrated in Figure 2. It should be pointed out that, the value of the Richardson number provides a measure of the importance of buoyancy-driven natural convection relative to the lid-driven forced convection. For $Ri = 0.01$ ($Ri < 1$), Figure 2 shows that the flow is bicellular symmetric for this small value of Ri for which the buoyancy effects are overwhelmed by the forced flow imposed by the movement of the driven walls. For this case, the fluid is mainly driven by the shear forces generated by the movement of the side walls since the effect of the buoyancy forces is negligible. Indeed, the hot/(cold)fluid near the hot/(cold) vertical wall is driven by the movement of the right/(left) wall with the same speed as that of the cold/(hot)fluid (same kinetic energy) in the same direction. This situation leads to the formation of two counter-rotating cells with comparable sizes and intensities. Note that each vertical wall imposes the direction of rotation to the neighboring cell. The intensities of the both cells $\psi_{\max}/|\psi_{\min}|$ are

insensitive to the presence of radiation, they are 0.0896/0.0908 for $\varepsilon = 0$ and 1. Regarding the thermal behavior, it can be seen from Figure 2 that the field of isotherms is characterized by asymmetry with respect to the central vertical axis of the cavity. In addition, two isothermal zones (each having the temperature of the neighboring active wall) are formed near the upper corners of the cavity, imposing an obvious curvature to the peripheral isotherms beneath the upper adiabatic wall. Consequently, the isotherms become very tight in the upper central part of the cavity for $\varepsilon = 0$. This important heat exchange at this part of the cavity results from the first contact between the peripheral lines of the cooled and heated cells located respectively in the left and right halves of the cavity. It should be noted that for this week value of Ri, the radiation of the walls has no effect on the streamlines and the symmetry of the temperature field in maintained as a consequence of the domination of the forced convection regime. The only difference observed between the temperature fields obtained with $\varepsilon = 0$ and $\varepsilon = 1$ is the curvature exhibited by the isotherms in the presence of radiation ($\varepsilon = 1$) near the horizontal adiabatic walls instead of being normal to the latter for $\varepsilon = 0$.

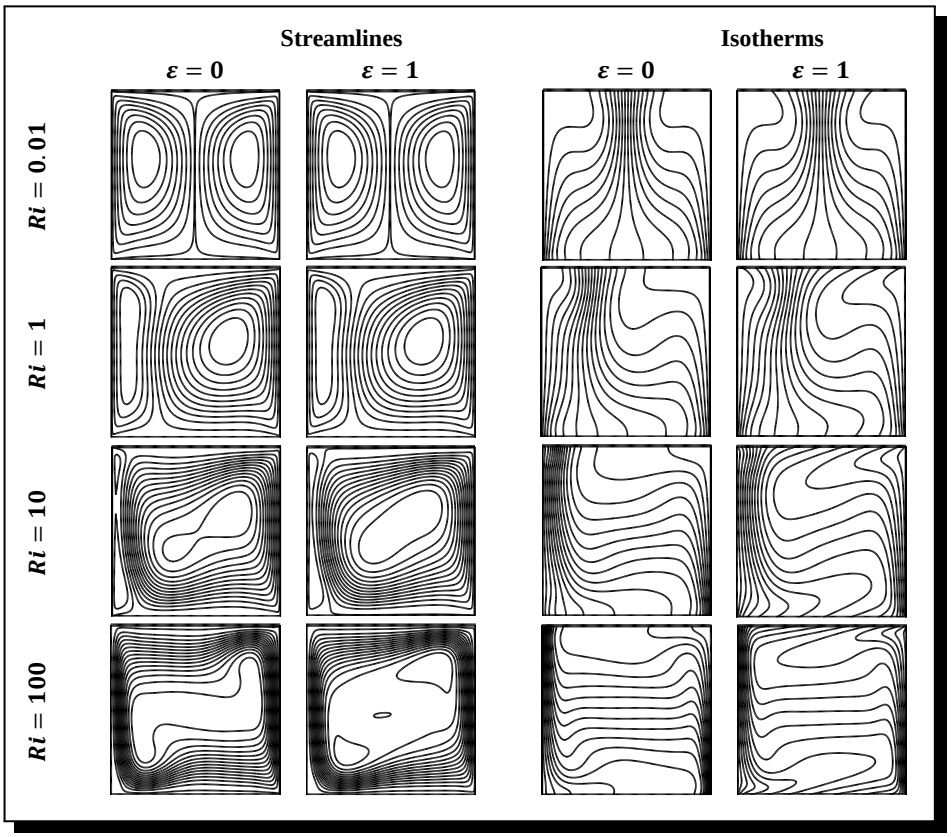

Figure 2. Streamlines (first and second columns) and isotherms (third and fourth columns) for different values of Ri and ε for $T'_0 = 293.5K$ and $\Delta T' = 10K$

For $Ri = 1$, the effect of natural convection due to the buoyancy forces becomes comparable to that of forced convection engendered by the shear forces generated by the movement of the vertical walls. The examination of Figure 2, corresponding to $Ri = 1$, shows the presence of two cells of different size, one counter-clockwise rotating (the right one) and the second

clockwise rotating (the left one). The destruction of the symmetry observed for $Ri = 0.01$ is destructed in favor the right cell. The latter becomes more voluminous and more intense than the left one, due the fact that the buoyancy and shear forces are aiding each other near the heated wall while their effects are antagonistic near the cold wall. Consequently, the competition between the buoyancy and shear forces at the cold wall leads to a weakening of the positive cell due to the involved antagonistic forces. The reduction of the left cell's size occurs under the expansion of the negative right cell that, on the contrary, benefits from the aiding effects of buoyancy and shear forces at the heated wall and expands to cover about 70% of the cavity space. For $Ri = 1$, the presence of radiation has a negligible qualitative effect on the flow structure but acts positively on its intensity. Indeed, the intensity $\psi_{\max}/|\psi_{\min}|$ goes from 0.0477/0.1185 to 0.0490/0.1216 when ε increases from 0 to 1, which corresponds to a moderate improvement of about 2.73%/2.62% following this increase of ε. Moreover, by incrementing Ri from 0.01 to 1, the intensity $\psi_{\max}/|\psi_{\min}|$ decreases/increases by about 46.8%/30.5% for $\varepsilon = 0$ and decreases/increases by about 45.3%/34% for $\varepsilon = 1$.

The examination of the associated temperature field in Figure 2 shows that the symmetry observed for $Ri = 0.01$ is destroyed for $Ri = 1$ under the increasing effect of the buoyancy forces. The area with strong thermal gradients between the two cells is moved to the left (toward the cold wall) and the vertical walls play a more active role. In addition, the effect of radiation on the isotherms is more obvious and shows a tendency to reduce the thermal gradients and make the temperature distribution more uniform inside the cavity.

Based on the role played by the shear and buoyancy forces near the active boundaries, it becomes easy to expect the impact of these forces on the flow structure. By increasing the value of Ri above 10, the narrow positive cell aligned with the cold wall is further crushed under the effect of the expansion of the negative cell. In fact, the increase of the buoyancy forces due to the increase of Ri in addition to the complicity of the shear ones act in supporting the negative cell (the right dominating one) that becomes completely dominant. Globally, in the regime dominated by the buoyancy forces, the increase of Ri or ε affects mainly the shape of the internal streamlines, the intensity of the flow and leads to an enlargement of the stagnant zone. Concerning the thermal aspect of the problem, the distribution of temperature inside the cavity for $\varepsilon = 0$ is characterized by a stratification of the isotherms (supported by the increase of Ri), leading in the case of dominating natural convection regime ($Ri = 100$) to zero gradients in the central part of the cavity. In addition, the increase of Ri reinforces the existence of two thermal boundary layers on the active walls. For $\varepsilon = 1$, the effect of radiation on the thermal field is more manifest. By increasing Ri, the isotherms are more and more inclined at the horizontal adiabatic walls but tend to become horizontal in the central part of the cavity.

For additional information on the effect of the governing parameters, the profiles of the vertical velocity component at mid-height of the cavity are plotted in Figure 3a ($\varepsilon = 0$) and Figure 3b ($\varepsilon = 1$) for different values of Ri. It can be seen from these figures that these profiles are well affected by the variation of Ri. In the regime dominated by forced convection, the profile of velocity exhibits a minimum near the center of the cavity (around $X = 0.46$) but, in the dominating natural convection regime, the velocity vanishes over a range of X containing the

center of the cavity and widens slightly by increasing Ri. More specifically, Figure 3 show that the velocity of the fluid is practically zero in the range $0.36 < X < 0.7/(0.4 < X < 0.67)$ for $\varepsilon = 0/(1)$ and $Ri > 1$. Moreover, each profile exhibits two peaks of velocity for $Ri \geq 10$ that intensify while moving toward the vertical walls by increasing Ri. For the highest value of Ri, the maximum $V_{max} = 2.67/(V_{max} = 2.89)$ and minimum $V_{min} = -2.65/(V_{min} = -2.86)$ values reached near the active walls for $\varepsilon = 0/(1)$ exceed largely the value imposed to the moving walls ($V = 1$).

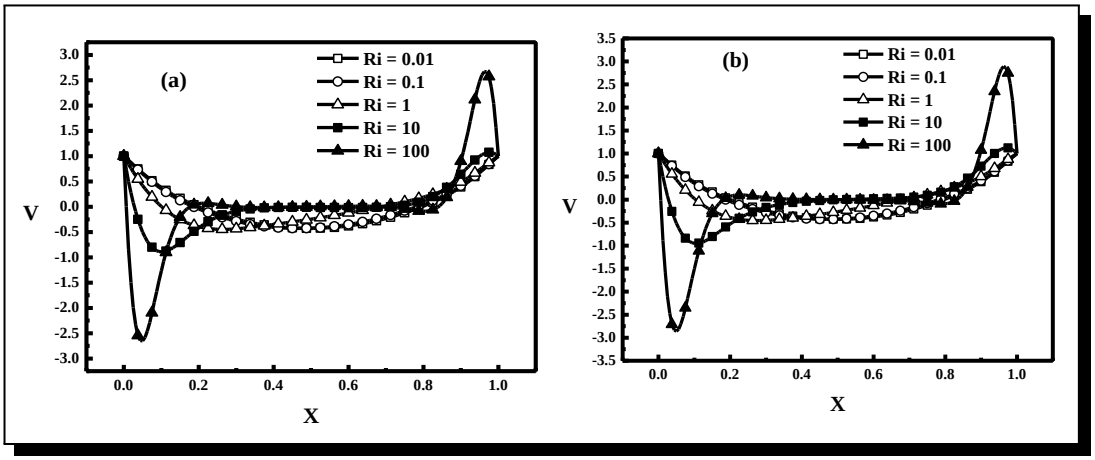

Figure 3. Vertical velocity profiles at mid-height of the cavity for (a) $\varepsilon = 0$ and (b) $\varepsilon = 1$ and different values of Ri

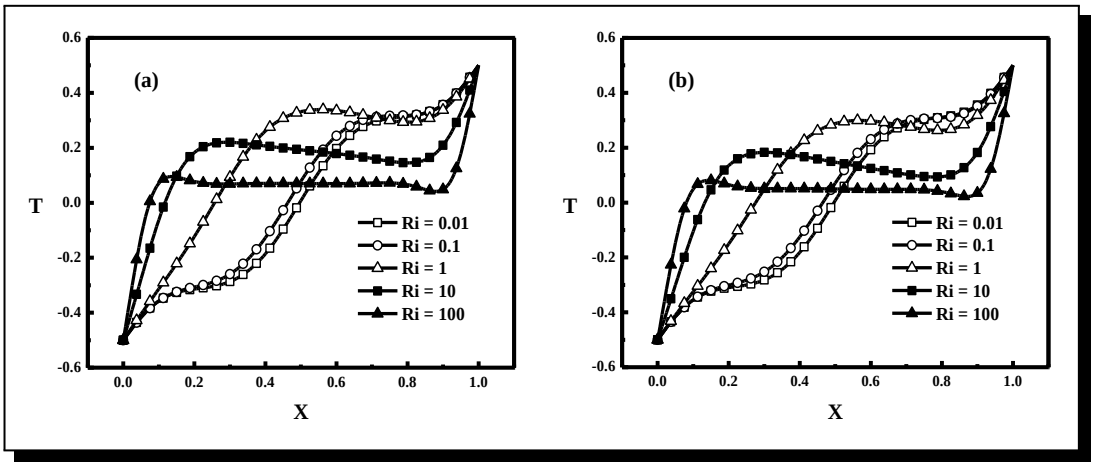

Figure 4. Temperature profiles at mid-height of the cavity for (a) $\varepsilon = 0$ and (b) $\varepsilon = 1$ and different values of Ri

For the same objective but concerning the thermal aspect of the problem, the temperature profiles at mid-height of the cavity are exemplified in Figure 4a ($\varepsilon = 0$) and Figure 4b ($\varepsilon = 1$) for various values of Ri. In the absence of radiation and dominating forced convection regime ($Ri < 1$), it can be seen that the temperature profile is quasi-linear in the range $0.34 < X < 0.64$ and exhibits a plateau around $T \approx 0.3$ for $0.7 < X < 0.82$. In mixed convection regime ($Ri = 1$), the linear profile of the temperature is shifted in the range $0 < X < 0.44$. The behavior changes drastically when natural convection is the dominating regime ($Ri > 1$). In fact, the temperature

evolution becomes linear near both the active walls, which confirms the formation of thermal boundary layers in the ranges $0 < X < 0.1$ and $0.9 < X < 1$. Out of these ranges, the temperature is almost constant ($T \approx 0$),confirming the stratification of the isotherms observed in Figure 2 for $Ri = 100$. The presence of the radiation, illustrated with $\varepsilon = 1$ in Figure 4b, shows a limited qualitative effect on the temperature profiles compared to those of $\varepsilon = 0$.

3.2 Heat Transfer

Variations versus the Richardson number Ri, of the average Nusselt numbers, resulting from contributions of convection, Nu_{Cv}, and radiation, Nu_{Rd}, and the total Nusselt number, Nu, evaluated along the hot wall are presented in Figure 5 for $\varepsilon = 1$. Regarding the overall behavior, Figure 5 shows a monotonous increase of Nu_{Cv}, Nu_{Rd} and Nu with Ri. This tendency is expected since the increase of Ri is known to promote the flow intensification. Figure 5 shows also that the contribution of radiation to the total heat transfer is lower than that of convection for $Ri < 1$ where the shear forces outclass the buoyancy ones in the forced convection regime. From the threshold value around $Ri = 1$, the tendency is inverted in favor of the radiative component of Nusselt number in terms of contribution to the total heat transfer. As indication, at $Ri = 0.01$ ($Ri = 100$), Nu_{Cv} represents 78.6%/(36.8%) of Nu_{Rd}. In addition, from this threshold value, Nu_{Rd} increases with a faster rate than that of Nu_{Cv} by incrementing Ri. Behavior can be explained by the increase of the convective component with Gr (contribution of the buoyancy effect by increasing Ri through the incrementation of the Grashof number) and the radiative component with Gr via N_r (the increase in the actual dimension of the cavity).

Finally, Figure 5 shows also that the effect of radiation on Nu is positive and its importance is reinforced by increasing ε, particularly in the range of Ri where the buoyance forces play a non-negligible role. Quantitatively, for $\varepsilon = 1$, the value of $Nu_{Cv}/Nu_{Rd}/Nu$ is multiplied by 3.48/22/7.43 by increasing Ri from 0.01 to 100.

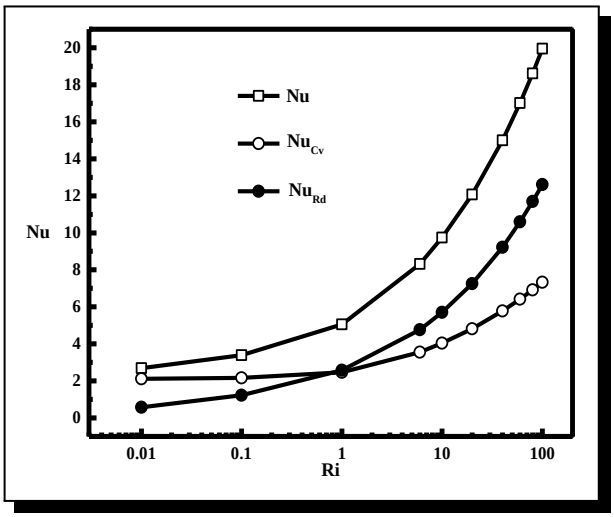

Figure 5. Variations of Nusselt numbers vs. Ri for $\varepsilon = 1$, $T_0' = 293.5\,\mathrm{K}$ and $\Delta T' = 10\,\mathrm{K}$

.

4. Conclusions

Mixed convection and radiation effect in a two-sided lid-driven enclosure is studied by using LBM simulation. The parameters governing the problem are the emissivity of the walls, ε ($0 \leq \varepsilon \leq 1$), and the Richardson number, Ri ($0.01 \leq Ri \leq 100$), varied through the Grashof number, Gr, for fixed Reynolds number, Re ($Re = 100$). The main findings of the study are summarized as follows:

- At low Richardson numbers ($Ri \ll 1$), the flow structure is bicellular symmetric dominated by the forced convection mode. The radiation has no effect on the flow nature and the heat transfer in the cavity.
- At high Richardson numbers ($Ri \sim 100$), the buoyancy forces are much more important than the shear forces and the flow is dominated by a monocellular structure.
- There is a thresholds of Ri above/below which convection heat transfer is lower/greater than radiative one.

Competing Interests

The authors declare that they have no competing interests.

Authors' Contributions

All the authors contributed significantly in writing this article. The authors read and approved the final manuscript.

References

[1] A. Al-Amiri and K. Khanafer, Fluid-structure interaction analysis of mixed convection heat transfer in a lid-driven cavity with a flexible bottom wall, *International Journal of Heat and Mass Transfer* **54** (2011), 3826 – 3836, DOI: 10.1016/j.ijheatmasstransfer.2011.04.047.

[2] M.A. Antar, R. Ben-Mansour and S.A. Al-Dini, The effect of thermal radiation on the heat transfer characteristics of lid-driven cavity with a moving surface, *International Journal of Numerical Methods for Heat & Fluid Flow* **24** (2014), 679 – 696, DOI: 10.1108/HFF-06-2012-0136.

[3] C. Balaji, M. Hölling and H. Herwig, Combined laminar mixed convection and surface radiation using asymptotic computational fluid dynamics (ACFD), *Heat and Mass Transfer / Waerme- Und Stoffuebertragung* **43** (2007), 567 – 577, DOI: 10.1007/s00231-006-0145-3.

[4] M.A. Belmiloud and N.E.S. Chemloul, Numerical study of mixed convection coupled to radiation in a square cavity with a lid-driven, *International Journal of Mechanical, Aerospace, Industrial, Mechatronic and Manufacturing Engineering International Scholarly and Scientific Research & Innovation* **9** (2015), 1815 – 1821, DOI: 10.5281/zenodo.1109928.

[5] P.L. Bhatnagar, E.P. Gross and M. Krook, A model for collision processes in gases. I. Small amplitude processes in charged and neutral one-component systems, *Physical Review* **94** (1954), 511 – 525, DOI: 10.1103/PhysRev.94.511.

[6] S. Chapman, T.G. Cowling and D. Park, The mathematical theory of non-uniform gases, *American Journal of Physics* **30** (1962), 389 – 389, DOI: 10.1119/1.1942035.

[7] Y. Dahani, M. Hasnaoui, A. Amahmid, A. El Mansouri and S. Hasnaoui, Lattice Boltzmann simulation of combined effects of radiation and mixed convection in a lid-driven cavity with cooling and heating by sinusoidal temperature profiles on one side, *Heat Transfer Engineering* **41** (2020), DOI: 10.1080/01457632.2018.1558009.

[8] Y. Guo, R. Bennacer, S. Shen, D.E. Ameziani and M. Bouzidi, Simulation of mixed convection in slender rectangular cavity with lattice Boltzmann method, *International Journal of Numerical Methods for Heat & Fluid Flow* **20** (2010), 130 – 148, DOI: 10.1108/09615531011008163.

[9] H. Hottel and A. Saroffim, *Radiative Heat Transfer*, McGraw-Hil, New York (1967).

[10] O.J. Ilegbusi and M.D. Mat, A comparison of predictions and measurements of kinematic mixing of two fluids in a 2D enclosure, *Applied Mathematical Modelling* **24** (2000), 199 – 213, DOI: 10.1016/S0307-904X(99)00029-3.

[11] R. Iwatsu, J.M. Hyun and K. Kuwahara, Mixed convection in a driven cavity with a stable vertical temperature gradient, *International Journal of Heat and Mass Transfer* **36** (1993), 1601 – 1608, DOI: 10.1016/S0017-9310(05)80069-9.

[12] J.R. Koseff and R.L. Street, Visualization studies of a shear driven three-dimensional recirculating flow, *Journal of Fluids Engineering* **106** (1984), 21 – 27, DOI: 10.1115/1.3242393.

[13] L. Luo, *Lattice-gas automata and lattice Boltzmann equations for two-dimensional hydrodynamics*, Georgia Institute of Technology (1993), `http://adsabs.harvard.edu/abs/1993PhDT.....233L`.

[14] S.K. Mahapatra, Mixed convection inside a differentially heated enclosure and its interaction with radiation-an exhaustive study, *Heat Transfer Engineering* **35** (2014), 74 – 93, DOI: 10.1080/01457632.2013.730912.

[15] C. Migeon, G. Pineau and A. Texier, Three-dimensionality development inside standard parallelepipedic lid-driven cavities at $Re = 1000$, *Journal of Fluids and Structures* **17** (2003), 717 – 738, DOI: 10.1016/S0889-9746(03)00009-4.

[16] R.D. Mills, On the closed motion of a fluid in a square cavity, *The Aeronautical Journal* **69** (1965), 116 – 120, DOI: 10.1017/S0001924000060371.

[17] M. Mohammadi and S.A.G. Nassab, effect of radiation on mixed convection inside a lid-driven square cavity with various optical thicknesses and Richardson numbers, *Heat Transfer Engineering* **38** (2017), 653 – 665, DOI: 10.1080/01457632.2016.1200386.

[18] A.A. Mohammed, *Lattice Boltzmann Method: Fundamentals and Engineering Applications with Computer Codes*, Springer-Verlag, London (2012), DOI: 10.2514/1.J051744.

[19] R. Nasrin, Influences of physical parameters on mixed convection in a horizontal lid-driven cavity with an undulating base surface, *Numerical Heat Transfer, Part A: Applications* **61** (2012), 306 – 321, DOI: 10.1080/10407782.2012.647987.

[20] D.A. Perumal, Lattice Boltzmann computation of multiple solutions in a double-sided square and rectangular cavity flows, *Thermal Science and Engineering Progress* **6** (2018), 48 – 56, DOI: 10.1016/j.tsep.2017.10.009.

[21] A.K. Prasad and J.R. Koseff, Combined forced and natural convection heat transfer in a deep lid-driven cavity flow, *International Journal of Heat and Fluid Flow* **17** (1996), 460 – 467, DOI: 10.1016/0142-727X(96)00054-9.

[22] M.J. Vogel, A.H. Hirsa and J.M. Lopez, Spatio-temporal dynamics of a periodically driven cavity flow, *Journal of Fluid Mechanics* **478** (2003), 197 – 226, DOI: 10.1017/S002211200200349X.

[23] L. Wang, B. Shi, Z. Chai and X. Yang, Regularized lattice Boltzmann model for double-diffusive convection in vertical enclosures with heating and salting from below, *Applied Thermal Engineering* **103** (2016), 365 – 376, DOI: 10.1016/j.applthermaleng.2016.04.080.

[24] H. Wang, S. Xin and P. Le Quéré, Étude numérique du couplage de la convection naturelle avec le rayonnement de surfaces en cavité carrée remplie d'air, *Comptes Rendus - Mecanique* **334** (2006), 48 – 57, DOI: 10.1016/j.crme.2005.10.011.

[25] Q. Zou and X. He, On pressure and velocity boundary conditions for the lattice Boltzmann BGK model, *Physics of Fluids* **9** (1997), 1591 – 1598, DOI: 10.1063/1.869307.